Wang, K., Suchkov, S. V., Titchener, J. G., Szameit, A., & Sukhorukov, A. A. (2019). Inline detection and reconstruction of multiphoton quantum states. *Optica*, *6*(1), 41-44. https://doi.org/10.1364/OPTICA.6.000041

Letter Vol. 6, No. 1 / January 2019 / Optica 41

Inline detection and reconstruction of multiphoton quantum states

Kai Wang,[1,2,*] Sergey V. Suchkov,[1] James G. Titchener,[1,3] Alexander Szameit,[2] and Andrey A. Sukhorukov[1]

[1]Nonlinear Physics Centre, Research School of Physics and Engineering, The Australian National University, Canberra ACT 2601, Australia
[2]Institute for Physics, Universität Rostock, Albert-Einstein-Str. 23, 18059 Rostock, Germany
[3]Quantum Technology Enterprise Centre, Quantum Engineering Technology Labs, H. H. Wills Physics Laboratory and Department of Electrical and Electronic Engineering, University of Bristol, Bristol BS8 1FD, UK
*Corresponding author: kai.wang@anu.edu.au

Received 14 August 2018; revised 30 November 2018; accepted 2 December 2018 (Doc. ID 342410); published 7 January 2019

Integrated single-photon detectors open new possibilities for monitoring inside quantum photonic circuits. We present a concept for the inline measurement of spatially encoded multiphoton quantum states, while keeping the transmitted ones undisturbed. We theoretically establish that by recording photon correlations from optimally positioned detectors on top of coupled waveguides with detuned propagation constants, one can perform robust reconstruction of the N-photon density matrix describing amplitude, phase, coherence, and quantum entanglement. We report proof-of-principle experiments using classical light, which emulates the single-photon regime. Our method opens a pathway towards practical and fast inline quantum measurements for diverse applications in quantum photonics.

https://doi.org/10.1364/OPTICA.6.000041

Quantum properties of multiple entangled photons underpin a broad range of applications [1–3] encompassing enhanced sensing, imaging, secure communications, and information processing. Accordingly, approaches for measurements of multiphoton states are actively developing, from conventional quantum tomography with multiple bulk optical elements [4] to integrated photonic circuits [5]. Whereas entangled photon states were traditionally measured at the output of photonic circuits, the capability to measure the state within the circuits could enable direct monitoring of their operation and pinpointing possible issues in real-time.

Latest advances in nanofabrication enable the integration of multiple single-photon detectors based on superconducting nanowires [6,7], opening new possibilities for photon monitoring inside photonic circuits [8]. However, there remains an open question of how to perform inline measurements of the quantum features of multiphoton states encoded in their density matrices, while ideally keeping the transmitted states undisturbed apart from weak overall loss. Such capability would be highly desirable similar to the classical analogues [9], yet it presents a challenging problem since traditional approaches for quantum measurements are not suitable. In particular, direct measurement methods [10,11] are difficult to employ due to complex measurement operators. On the other hand, conventional state tomography [4], a most widely used reconstruction method, requires reconfigurable elements to apply modified projective measurements in different time windows. Recently, the reconstruction was achieved in static optical circuits [12–14] or metasurfaces [15]; however, it comes at a cost of spreading out quantum states to a larger number of outputs, which is incompatible with the inline detection principle.

In this work, we present a new conceptual approach for practical inline measurement of multiphoton states using integrated detectors, which is suitable for multiport systems. We employ a new regime of correlation measurements among detectors at different propagation stages associated with the same static Hamiltonian, taking the unique advantage of photons in waveguides implementing gradually coupled transformations. We illustrate it for two waveguides in Fig. 1(a). The coupled waveguides (coupling coefficient C) have different propagation constants (detuned by $\pm\beta$), and the length L is exactly a revival period. An even number M of weakly coupled single-photon click detectors are placed at $M/2$ cross sections, starting from z_1 with equal distances $2L/M$ between each other. As we demonstrate in the following, the measurement of N-fold nonlocal correlations by averaging the coincidence events enables a full reconstruction of the density matrix ρ_N for N-photon states.

The quantum state evolution along the waveguides, under the assumption of weakly coupled detectors, is governed by the Hamiltonian

$$\hat{H} = \beta\hat{a}_1^\dagger\hat{a}_1 - \beta\hat{a}_2^\dagger\hat{a}_2 + C\hat{a}_1^\dagger\hat{a}_2 + C\hat{a}_2^\dagger\hat{a}_1, \tag{1}$$

where $\hat{a}_q^\dagger(\hat{a}_q)$ are the photon creation (annihilation) operators in waveguide number q. We use Heisenberg representation [16,17] and map time t to the propagation distance $-z$. Hence, the operator evolution reads

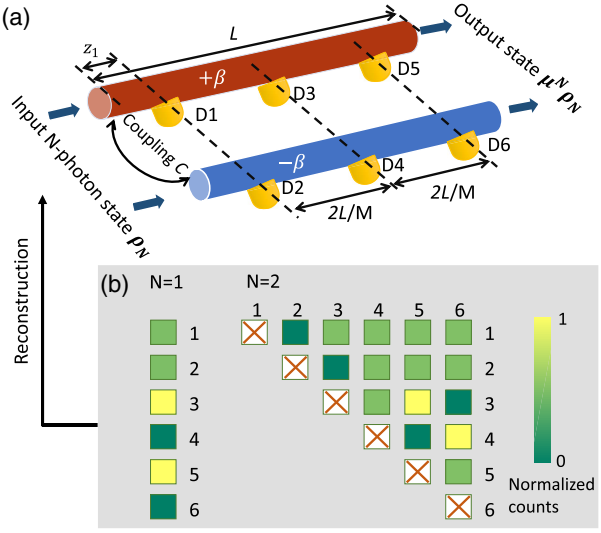

Fig. 1. Conceptual sketch of inline detection and reconstruction of N-photon state ρ_N with two spatial modes. (a) Two waveguides with coupling constant C and detuning $\pm\beta$ in propagation constants. An even number M of single-photon click detectors are positioned at $M/2$ equidistant cross sections, illustrated for $M = 6$ with D1–D6 labels. (b) Examples of simulated single-photon counts ($N = 1$) and N-fold correlations (for $N = 2$) for $z_1 = 0$ and $\beta = C/\sqrt{2}$, which enable full reconstruction of the input density matrix ρ_N.

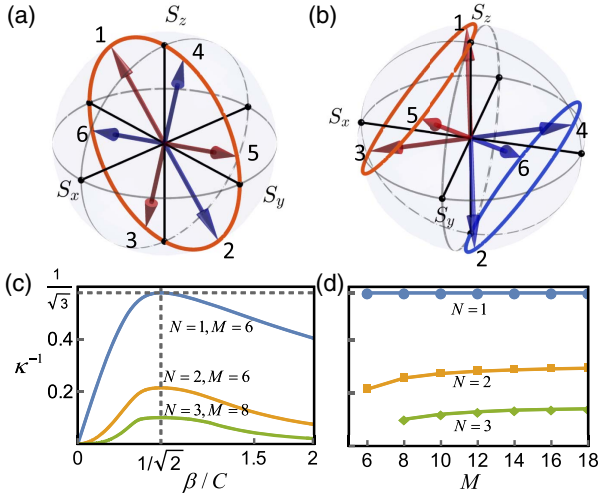

Fig. 2. Robust reconstruction with waveguide detuning. (a,b) The analysis states on a Bloch sphere for (a) identical waveguides ($\beta = 0$) and (b) introduced detuning ($\beta = C/\sqrt{2}$). Curves show the evolution along z, and arrows correspond to six detectors as indicated in Fig. 1(a). The $M = 6$ analysis states consist of three pairs of orthogonal ones, with each pair indicated by two arrows pointing in opposite directions. Red and blue colors denote waveguides 1 and 2, respectively. (c,d) Inverse condition number κ^{-1} versus (c) normalized detuning β/C and (d) number of detectors M for the optimal detuning $\beta = C/\sqrt{2}$.

$$\hat{a}_q(z) = \sum_{q'=1,2} \mathbf{T}^*_{q,q'}(z)\hat{a}_{q'}(0),$$
$$\hat{a}^\dagger_q(z) = \sum_{q'=1,2} \mathbf{T}_{q,q'}(z)\hat{a}^\dagger_{q'}(0). \quad (2)$$

Here, the linear transfer matrix elements of the waveguide coupler are $\mathbf{T}_{q,q}(z) = \cos(\eta z) + i(-1)^q\beta\eta^{-1}\sin(\eta z)$ and $\mathbf{T}_{q,3-q} = -iC\eta^{-1}\sin(\eta z)$, where $\eta = (C^2+\beta^2)^{1/2}$. We note that the input state is restored at the revival length $L = 2\pi/\eta$, since $\hat{a}^\dagger_q(L) = \hat{a}^\dagger_q(0)$. While the inline detectors introduce small loss, due to their symmetric positions, the revival effect will remain, and the output N-photon density matrix would only exhibit an overall scaling $\mu^N\rho_N$, where μ is a one-photon transmission coefficient, which can be close to unity [for details, see Supplement 1 Section S3].

We consider the measurement of states with a fixed photon number N, which is a practically important regime [4,12–14]. The reconstruction can also be performed when the maximum photon number is known (see Supplement 1 Section S1) [18]. We base the analysis on the most common type of click detectors that cannot resolve the number of photons arriving simultaneously at the same detector, and cannot distinguish which photon is which. Nevertheless, our design is also compatible with number-resolvable detectors and a distinguishable detection scheme (for details see Supplement 1 Section S1). If either zero or one photon (but not more) are incident on detector m, then the general positive-operator valued measure (POVM) detection operator [19] can be represented as $\hat{A}_m = \hat{a}^\dagger_{q_m}(z_m)\hat{a}_{q_m}(z_m)$, where q_m is the waveguide number and z_m is the detector coordinate. Accordingly, the photon correlations corresponding to the simultaneous detection of N photons by a combination of N detectors with numbers $m_1, m_2, \ldots, m_N$, such that there is at most one photon at each detector, are

$$\Gamma(m_1, m_2, \ldots, m_N) = \mathrm{Tr}(\rho_N \hat{A}_{m_1}\hat{A}_{m_2}\cdots\hat{A}_{m_N}). \quad (3)$$

For a single photon ($N = 1$), the measurement corresponds to a direct accumulation of counts at each detector without correlations, and we show an example in Fig. 1(b, left) for a pure input state $|\psi\rangle = [1,1]^T/\sqrt{2}$ with the density matrix $\rho_1 = |\psi\rangle\langle\psi|$. We present an example of coincidence counts for a two-photon N00N state [19] ($N = 2$) in Fig. 1(b, right), corresponding to the events of clicks at different combinations of two detectors.

We outline the principle of reconstructing the input N-photon density matrix ρ_N from the correlation measurements. The vectors $|\psi_q\rangle = [\mathbf{T}_{q,1}, \mathbf{T}_{q,2}]^T$ are the analysis states, which define the measurements at the different detector positions. We visualize their evolution along z on a Bloch sphere, where the projector $|\psi_q\rangle\langle\psi_q|$ is decomposed into the Pauli matrices $\hat{\sigma}_i (i = x, y, z)$ to generate the coordinates $S_i = \mathrm{Tr}(\hat{\sigma}_i|\psi_q\rangle\langle\psi_q|)$. First, we present the trajectories for the case of no detuning ($\beta = 0$) in Fig. 2(a), where we see that the analysis states simply trace out a circle along the Bloch sphere. Considering for example $M = 6$ detectors as sketched in Fig. 1(a), all the analysis states corresponding to detectors shown by arrows are in one plane. Such a configuration cannot probe states beyond that plane; therefore, one cannot perform state reconstruction with a static, nondetuned directional coupler. In contrast, for detuned waveguides ($\beta \neq 0$), the circular trajectories in the first and second waveguides become nondegenerate [see the red and blue curves in Fig. 2(b)]. We indicate the analysis states with arrows for $M = 6$, and note that they are spread out to different directions in the sphere and can thus be utilized to probe all information about the states and enable the density matrix reconstruction.

The input state reconstruction is performed as follows. First, we introduce an index $p = 1, 2, \ldots, P$ with $P = M!/[N!(M-N)!]$ to enumerate all possible N combinations of M detectors, $(m_1, m_2, \ldots, m_N)_p$. Second, we select $S = (N+3)!/(N!3!)$

real-valued parameters $r_1, r_2, \ldots, r_S$, representing independent real and imaginary parts of the density matrix elements following the procedure in the Supplementary Material of Ref. [14]. Here, we consider the indistinguishable detection scheme that does not tell which photon is which, and formulate Eq. (3) in a matrix form,

$$\Gamma_p \equiv \Gamma(m_1, m_2, \ldots, m_N)_p = \sum_{s=1}^{S} \mathbf{B}_{p,s} r_s, \tag{4}$$

where the elements of the instrument matrix $\mathbf{B}$ are expressed through the transfer matrices $\mathbf{T}$ at the detector positions. The minimum requirement for the density matrix parameters $\{r_s\}$ to be reconstructed from the correlations by performing pseudoinversion of Eq. (3) is $P \geq S$, i.e., when the number of detectors

$$M \geq N + 3. \tag{5}$$

We now analyze the robustness of reconstruction with respect to possible experimental inaccuracies in the correlation measurements, such as shot noise. This can be quantified by the condition number κ of the matrix $\mathbf{B}$ (see Refs. [14,20] and Supplement 1 Section S2 for details). Then, the most accurate reconstruction corresponds to the smallest condition number. We numerically calculate the condition numbers for different combinations of M and N, considering a symmetric arrangement of detectors, as sketched in Fig. 1(a). We find that accurate reconstruction can be achieved for the number of click detectors $M > N + 3$. However, the condition number is infinite, and the reconstruction cannot be performed for $M = N + 3$. This happens because the M analysis states are not fully independent, but actually constitute $M/2$ pairs of orthogonal states, as illustrated in Fig. 2(b). There is no contradiction with Eq. (5), since the latter establishes only an ultimate lower bound for reconstruction.

We determine that a detuning of the waveguide propagation constants (β) is essential to perform the reconstruction. We illustrate in Fig. 2(c) that the variation of β strongly changes the reconstruction condition for a different number of photons $N = 1, 2, 3$, considering the minimum possible even number of detectors. With no detuning, for $\beta = 0$, κ^{-1} goes to zero, meaning that the reconstruction is ill-conditioned and cannot be performed in practice. The optimal measurement frames occur at $\beta/C \simeq 1/\sqrt{2}$. In Fig. 2(d), we fix $\beta/C = 1/\sqrt{2}$ and plot κ^{-1} versus the number of detectors M. We find that $\kappa^{-1} = 1/\sqrt{3}$ for $N = 1$ and any $M \geq 6$, in agreement with classical measurement theory [20]. Importantly, an optimal condition number can also be preserved for stronger couplings to the detectors, when the detection rate is enhanced at a cost of losing more photons in the output (see Supplement 1 Section S3 for details). The post-fabricated device can be calibrated and described by a transfer matrix, which thereby accounts for fabrication imperfections and different detection efficiencies and enables accurate reconstructions, provided the condition number is close to optimal, without a need to characterize individual structure parameters (see Supplement 1 Section S4).

We demonstrate the scheme with *proof-of-principle experiments* for classical light. Mathematically, this is equivalent to the single-photon problem [17,21], since monochromatic laser light can be described by a density matrix of the same dimensionality as for a single photon, 2×2 corresponding to two waveguides. We employ laser-written waveguides in fused silica to perform a reconstruction with a source of coherent laser light. In the fabrication process, we use different laser energies to write the coupled waveguides, and thereby achieve a predetermined offset ($\pm\beta$) of the propagation constants for the fundamental modes in the two waveguides [22]. We launch 633 nm laser light into one of the waveguides and perform inline measurements of the evolution of intensity by observing the fluorescence (around 650 nm wavelength) emitted from color centers of the glass material under a microscope [22,23]. We present a characteristic fluorescence image in Fig. 3(a, top), which features a clear beating pattern due to light coupling between the waveguides along the propagation direction z. The extracted normalized power in each waveguide is shown in Fig. 3(a, bottom). We observe a good agreement with the theory (dashed line) for the coupled waveguide modes with $C = 0.0885$ mm^{-1} and propagation constants detuning $\beta = 0.0240$ mm^{-1}, corresponding to a single-photon condition number $\kappa = 2.8$. The observation of emitted fluorescence is conceptually equivalent to putting many weakly coupled detectors homogeneously along both waveguides.

We then test our reconstruction method using the fluorescence image of the waveguide coupler. In the 80-mm-long section of the fabricated structure shown in Fig. 3(a), light periodically couples several times between the waveguides. We truncate a section along z with one revival period L to mimic the inline quantum detection. Then, the state $\rho(z)$ can be predicted by the coupled wave equation using the characterized parameters as described above. We consider different z as starting positions, which allows us to effectively change the input state. We employ a maximum-likelihood method to perform a pseudoinversion of Eq. (4) and thereby find an input

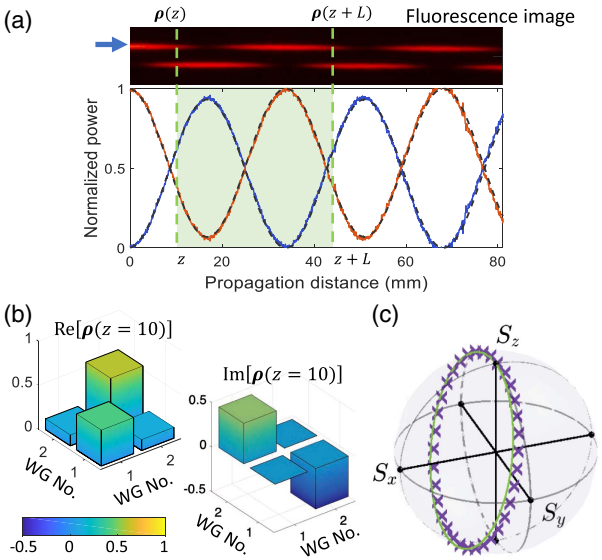

Fig. 3. Experimental inline measurement and reconstruction of $N = 1$ states emulated with classical laser light in detuned directional couplers. (a) A fluorescence image (top), showing light intensity along the coupler. Bottom, the corresponding normalized power evolution in each waveguide (solid curves) compared to theory (dashed curves). Shading indicates a section $(z, z + L)$, where inline measurements are used to reconstruct the full density matrix at the section input, $\rho(z)$. (b) The reconstructed real and imaginary parts of the density matrix elements for different combinations of the waveguide numbers (WG No.) at $z = 10$ mm, the beginning of the shaded section in (a). (c) Experimentally reconstructed $\rho(z)$ from a set of different positions z (crosses) compared with theoretical predictions (green curve) on a Bloch sphere, demonstrating an average fidelity of 99.65%.

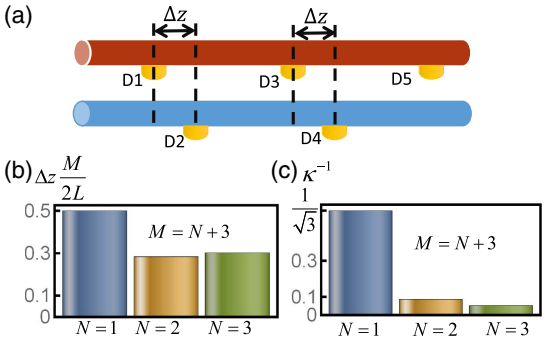

Fig. 4. Minimization of detector numbers to the limit $M = N + 3$. (a) Conceptual sketch of introducing a shift Δz for all detectors in one waveguide and skip the last detector if M is an odd number. (b) Normalized Δz (to $2L/M$) that achieves the best reconstruction condition with $\beta = C/\sqrt{2}$ for $N = 1, 2, 3$. (c) The corresponding inverse condition number for the three cases in (b).

density matrix that best fits the evolution of the fluorescence power in the two waveguides [see an example in Fig. 3(b)]. We analyze 34 different input states, truncated from successive z with 1 mm increments. The reconstructed states are plotted on a Bloch sphere with crosses in Fig. 3(c), and compared to theoretical modeling shown with a green curve. The coordinates are obtained via decomposing the density matrices to the Pauli matrices, i.e., $S_i = \mathrm{Tr}(\hat{\sigma}_i \rho)$ with i spanning x, y, z. We observe an excellent consistency between direct theoretical modeling and reconstruction from the experimental fluorescence images of the full density matrix, where we reach a very high average fidelity of 99.65%. This shows that reliable reconstructions are possible with a reasonable nonzero detuning, where the condition number of reconstruction and shot noise act as fundamental limits.

Finally, we explore the possibility to perform reconstruction with the minimal number of detectors, $M = N + 3$ according to Eq. (5). We perform extensive numerical modeling by optimizing β and the individual positions of all detectors. Although asymmetric positions may lead to a slight modification of the output state, this could be minimized by reducing the detector coupling. We find that well-conditioned reconstruction with $M = N + 3$ can be achieved for $N = 1, 2, 3$ with the detuning $\beta/C = 1/\sqrt{2}$ and by shifting all detectors in one waveguide by Δz, as sketched in Fig. 4(a) for $N = 2$ and $M = 5$. We present in Fig. 4(b) the optimal shifts Δz, normalized to the separation $2L/M$ between neighboring detectors in a waveguide. The corresponding inverse condition numbers are shown in Fig. 4(c). For $N = 1$, the best case appears at $\Delta z M/2L = 0.5$. For multiphoton states with $N = 2, 3$, the optimal values of Δz correspond to asymmetric detector positions, while the inverse condition numbers are lower (worse) compared to larger detector numbers [cf. Fig. 2(d)]. We note that for higher photon numbers $N \geq 4$, reconstruction with $M = N + 3$ appears impossible for any detector positions. Nevertheless, for a larger photon number N, one can use the configuration as in Fig. 1(a) with $M > N + 3$ to perform a reconstruction.

In conclusion, we proposed a practical and efficient approach for inline detection and measurement of single and multiphoton quantum states in coupled waveguides with integrated photon detectors, suitable for various applications in quantum photonics. We showed proof-of-principle results with laser-written waveguides for a classical light emulating single-photon regime. We presented the theory and experiments for a two-port system, and this can be scaled to multiple coupled waveguides. Moreover, our approach has a potential for translation from spatial to frequency and time-domain measurements using synthetic lattices in nonlinear waveguides [24].

Funding. Australian Research Council (ARC) (DP160100619); Australia-Germany Joint Research Cooperation Scheme; Erasmus+ (NANOPHI 2013 5659/002-001); Alexander von Humboldt-Stiftung; Deutsche Forschungsgemeinschaft (DFG) (BL 574/13-1, SZ 276/12-1, SZ 276/15-1, SZ 276/20-1, SZ 276/9-1).

See Supplement 1 for supporting content.

REFERENCES

1. A. Zeilinger, Phys. Scr. **92**, 072501 (2017).
2. C. Y. Lu, X. Q. Zhou, O. Guhne, W. B. Gao, J. Zhang, Z. S. Yuan, A. Goebel, T. Yang, and J. W. Pan, Nat. Phys. **3**, 91 (2007).
3. C. Reimer, M. Kues, P. Roztocki, B. Wetzel, F. Grazioso, B. E. Little, S. T. Chu, T. Johnston, Y. Bromberg, L. Caspani, D. J. Moss, and R. Morandotti, Science **351**, 1176 (2016).
4. D. F. V. James, P. G. Kwiat, W. J. Munro, and A. G. White, Phys. Rev. A **64**, 052312 (2001).
5. P. J. Shadbolt, M. R. Verde, A. Peruzzo, A. Politi, A. Laing, M. Lobino, J. C. F. Matthews, M. G. Thompson, and J. L. O'Brien, Nat. Photonics **6**, 45 (2012).
6. C. M. Natarajan, M. G. Tanner, and R. H. Hadfield, Supercond. Sci. Technol. **25**, 063001 (2012).
7. O. Kahl, S. Ferrari, V. Kovalyuk, A. Vetter, G. Lewes-Malandrakis, C. Nebel, A. Korneev, G. Goltsman, and W. Pernice, Optica **4**, 557 (2017).
8. W. H. P. Pernice, C. Schuck, O. Minaeva, M. Li, G. N. Goltsman, A. V. Sergienko, and H. X. Tang, Nat. Commun. **3**, 1325 (2012).
9. J. P. B. Mueller, K. Leosson, and F. Capasso, Optica **3**, 42 (2016).
10. J. S. Lundeen and C. Bamber, Phys. Rev. Lett. **108**, 070402 (2012).
11. G. S. Thekkadath, L. Giner, Y. Chalich, M. J. Horton, J. Banker, and J. S. Lundeen, Phys. Rev. Lett. **117**, 120401 (2016).
12. J. G. Titchener, A. S. Solntsev, and A. A. Sukhorukov, Opt. Lett. **41**, 4079 (2016).
13. D. Oren, M. Mutzafi, Y. C. Eldar, and M. Segev, Optica **4**, 993 (2017).
14. J. G. Titchener, M. Gräfe, R. Heilmann, A. S. Solntsev, A. Szameit, and A. A. Sukhorukov, npj Quant. Inform. **4**, 19 (2018).
15. K. Wang, J. G. Titchener, S. S. Kruk, L. Xu, H.-P. Chung, M. Parry, I. I. Kravchenko, Y.-H. Chen, A. S. Solntsev, Y. S. Kivshar, D. N. Neshev, and A. A. Sukhorukov, Science **361**, 1104 (2018).
16. Y. Bromberg, Y. Lahini, R. Morandotti, and Y. Silberberg, Phys. Rev. Lett. **102**, 253904 (2009).
17. A. Peruzzo, M. Lobino, J. C. F. Matthews, N. Matsuda, A. Politi, K. Poulios, X. Q. Zhou, Y. Lahini, N. Ismail, K. Worhoff, Y. Bromberg, Y. Silberberg, M. G. Thompson, and J. L. O'Brien, Science **329**, 1500 (2010).
18. O. Bayraktar, M. Swillo, C. Canalias, and G. Bjork, Phys. Rev. A **94**, 020105 (2016).
19. P. Kok and B. W. Lovett, *Introduction to Optical Quantum Information Processing* (Cambridge University, 2010).
20. M. R. Foreman, A. Favaro, and A. Aiello, Phys. Rev. Lett. **115**, 263901 (2015).
21. H. B. Perets, Y. Lahini, F. Pozzi, M. Sorel, R. Morandotti, and Y. Silberberg, Phys. Rev. Lett. **100**, 170506 (2008).
22. A. Szameit and S. Nolte, J. Phys. B **43**, 163001 (2010).
23. A. Szameit, F. Dreisow, H. Hartung, S. Nolte, A. Tunnermann, and F. Lederer, Appl. Phys. Lett. **90**, 241113 (2007).
24. B. A. Bell, K. Wang, A. S. Solntsev, D. N. Neshev, A. A. Sukhorukov, and B. J. Eggleton, Optica **4**, 1433 (2017).